


Large deviations in statistics of the convex hull of passive and active particles: A theoretical studySoheli Mukherjee^{*} and Naftali R. Smith[†]*Department of Environmental Physics, Blaustein Institutes for Desert Research, Ben-Gurion University of the Negev, Sede Boqer Campus, 8499000, Israel* (Received 28 November 2023; accepted 8 March 2024; published 8 April 2024)

We investigate analytically the distribution tails of the area A and perimeter L of a convex hull for different types of planar random walks. For N noninteracting Brownian motions of duration T we find that the large- L and $-A$ tails behave as $\mathcal{P}(L) \sim e^{-b_N L^2/DT}$ and $\mathcal{P}(A) \sim e^{-c_N A/DT}$, while the small- L and $-A$ tails behave as $\mathcal{P}(L) \sim e^{-d_N DT/L^2}$ and $\mathcal{P}(A) \sim e^{-e_N DT/A}$, where D is the diffusion coefficient. We calculated all of the coefficients (b_N, c_N, d_N, e_N) exactly. Strikingly, we find that b_N and c_N are independent of N for $N \geq 3$ and $N \geq 4$, respectively. We find that the large- L (A) tails are dominated by a single, most probable realization that attains the desired L (A). The left tails are dominated by the survival probability of the particles inside a circle of appropriate size. For active particles and at long times, we find that large- L and $-A$ tails are given by $\mathcal{P}(L) \sim e^{-T\Psi_N^{\text{act}}(L/T)}$ and $\mathcal{P}(A) \sim e^{-T\Psi_N^{\text{act}}(\sqrt{A}/T)}$, respectively. We calculate the rate functions Ψ_N exactly and find that they exhibit multiple singularities. We interpret these as DPTs of first order. We extended several of these results to dimensions $d > 2$. Our analytic predictions display excellent agreement with existing results that were obtained from extensive numerical simulations.

DOI: [10.1103/PhysRevE.109.044120](https://doi.org/10.1103/PhysRevE.109.044120)**I. INTRODUCTION****A. Background**

Brownian motion (BM) is a fundamental stochastic process that appears in many systems ranging from biology, physics, finance, computer science, and many more [1]. BM represents a broad universality class in the sense that for many models of random walks (RWs) and/or models of active particles—particles that generate dissipative, persistent motion by extracting energy from their surroundings [2–6]—the long-time typical behavior converges to that of a BM (passive). Examples of active matter arise in many biological systems like cellular tissue behavior [7], bacterial motion [8,9], formation of fish schools [10], and many more. Active particles exhibit a wide range of interesting behavior like non-Boltzmann stationary state [11,12], clustering at boundaries [13], jamming [14], etc. Different models of RWs and/or active particles are used to model various realistic systems such as movement of animals, self-propelled particles, polymers, etc.

The convex hull of a trajectory is the minimal convex set that contains all of the points along the trajectory. Convex hulls of stochastic trajectories have attracted much recent interest and they find many applications. For instance, they provide a natural way to define the home range of animals, which is the territory that the animal covers during a certain period of time. The area and perimeter of the convex hull thus gives a quantitative measurement of the home range [15,16]. Apart from the home range, the convex hull is a useful tool for

analyzing other phenomena, for instance to detect different phases in intermittent stochastic trajectories [17] or to study the spread of animal epidemics [18].

The mean perimeter and area of convex hull of a RW as a function of number of steps t is known (in the limit of large number of steps where it converges to BM) [19]. In the large- t limit, the mean perimeter and area scale as $\langle L \rangle \sim \sqrt{t}$ and $\langle A \rangle \sim t$, respectively. These results have been extended to many systems in the literature of physics [20–30] and mathematics [31–33]. For example, using the connection to extreme value statistics, exact results have been obtained for the mean perimeter and mean area for the convex hull of N noninteracting planar BMs [20,21]. In addition, the mean volume and surface area of the convex hull in arbitrary dimensions d has been calculated for a single BM and Brownian bridge [31–33], Levy processes [34], and a single BM in a confined geometry [35].

It is natural to try to give a more detailed characterization of the convex hull statistics beyond the average behaviors. Analytical calculations of the variance and higher-order moments of the distribution of these quantities are difficult [36]. To our knowledge, the only case for which an analytic result exists for the higher moments is for Brownian bridges [37], which is a BM constrained to end at its starting point. It is also called a “closed” BM (in contrast with the unconstrained “open” BM).

It is especially interesting and challenging to analytically understand the full distributions (including the large-deviation tails) of observables related to the convex hull (e.g., its perimeter or area). At present, they are rather poorly understood from an analytic point of view. One reason for this is that the convex hull constitutes a rather complex physical object, in the sense that it is affected, in a very nontrivial way,

^{*}soheli.mukherjee2@gmail.com[†]naftalismsith@gmail.com

by temporal correlations of the physical process. Fluctuations of the convex hull perimeter or area therefore depend on the nonequilibrium dynamics of the stochastic process. Moreover, these observables do not fall into one of the “standard” existing categories of observables (e.g., “dynamical observables” [38]) for which there exist generic theoretical frameworks for the study of large-deviation statistics.

In contrast, extensive numerical studies of the properties of convex hulls have been performed. These studies investigated not only the regime of typical fluctuations, but also used advanced importance-sampling techniques to probe far into the large-deviation regimes, describing convex hulls that are much larger or much smaller than average. The full distributions of the observables like area (A) and perimeter (L) in $d = 2$ dimensions, as well as their extensions to higher dimensions volume (V) and surface area (\mathcal{A}) have been numerically computed for different types of stochastic processes. These include the single planar BM or bridge [23], multiple BMs [24], BM in higher dimensions [25], self-avoiding RW [26,27], run and tumble particle (RTP) [28], and BM with resetting [29]. These numerical simulations were able to calculate the atypical fluctuations with probabilities that are in some cases extremely small, of order 10^{-1000} or even less. However, a comprehensive theory describing these numerical results is still lacking. Analytically there has been partial recent progress in mathematical literature for the “right” tails for the perimeter and area of a single random walker (under certain assumptions) [39,40].

In this paper, we calculate exactly the distribution of the tails of A , L , V and \mathcal{A} for different types of stochastic processes by studying the large deviation function (LDF) [38,41] encoding the dynamics. One of the important features of these LDFs that they may exhibit singularities which can be interpreted as dynamical phase transitions (DPTs) [42–49]. We consider both passive and active particles. We find that the physical picture in the right and left tails of the distributions is markedly different. As shown below, the right tails are dominated by a single, optimal large-scale trajectory of the process. In contrast, the left tails are dominated by realizations of the process that remain within a circle of appropriate size. The understanding of these physical pictures is what enables us to obtain the distribution tails analytically.

B. Model definitions

Let us now define precisely the theoretical models for which we aim to study the convex-hull area and perimeter distributions.

(i) *Brownian motion*. The motion of a BM in arbitrary dimension is described by the following Langevin equation:

$$\dot{\mathbf{r}}(t) = \sqrt{2D} \boldsymbol{\xi}(t), \quad (1)$$

where $\mathbf{r}(t)$ is the position of the particle at time t and $0 < t < T$, D is the diffusion constant, and $\boldsymbol{\xi}(t)$ are Gaussian white noises with $\langle \boldsymbol{\xi}(t) \rangle = 0$ and $\langle \xi_i(t) \xi_j(t') \rangle = \delta_{ij} \delta(t - t')$. Here $\langle \cdot \rangle$ denotes the ensemble average over realizations of the noise.

In $d = 2$, dimensional analysis yields the following scaling relations of the perimeter and the area distribution in the physical parameters (i.e., L , A , D ,

and T) [23]:

$$\mathcal{P}(L) = \frac{1}{\sqrt{DT}} P\left(\frac{L}{\sqrt{DT}}\right), \quad (2)$$

$$\mathcal{P}(A) = \frac{1}{DT} P\left(\frac{A}{DT}\right), \quad (3)$$

where the functions P and their arguments are dimensionless.

(ii) *Active particles*. A generic theoretical model for active particles can be written as

$$\dot{\mathbf{r}}(t) = \boldsymbol{\Sigma}(t), \quad (4)$$

where $\boldsymbol{\Sigma}(t)$ represents a noise term that originates in the self-propulsion of the particle with correlation time $1/\tau$. While most of our investigations for active particles will be quite general (under fairly mild assumptions as detailed below), for the sake of concreteness we will also give explicit results for particular models. Two of the most extensively studied models in $d = 2$ are active Brownian particle (ABP) [50] with the following equation of motion:

$$\dot{x} = v_0 \cos \theta(t), \quad \dot{y} = v_0 \sin \theta(t), \quad \dot{\theta} = \sqrt{2D_r} \eta(t), \quad (5)$$

where $\eta(t)$ is a Gaussian white noise with $\langle \eta(t) \rangle = 0$ and $\langle \eta(t) \eta(t') \rangle = \delta(t - t')$, v_0 is the constant speed of the particle and D_r is the rotational diffusion constant.

Another one is RTP [11] moving on the two-dimensional x - y plane,

$$\dot{\mathbf{r}}(t) = v_0 \boldsymbol{\sigma}(t), \quad (6)$$

where again v_0 is the constant speed of the particle and $\boldsymbol{\sigma}(t)$ is the colored noise. It is unit vector that reorients at some constant rate γ to a new orientation that is randomly chosen uniformly from the unit circle. Both of these models converge to BM in appropriate limits. For instance, for the RTP, in the limit $\gamma \rightarrow \infty$ and $v_0 \rightarrow \infty$, keeping the ratio $\frac{v_0^2}{2\gamma} = D_{\text{eff}}$ fixed (where D_{eff} is the effective diffusion coefficient), $\boldsymbol{\sigma}(t)$ becomes white noise and the typical fluctuations of the active models reduce to BM with diffusion coefficient $D = D_{\text{eff}}$ [51].

(iii) *Random walks*. One can also consider random walks that are discrete in time and/or in space [19,21–27]. As we will show below, our mathematical formalism that deals with active particles also addresses such random walks, under certain assumptions regarding the distribution of step sizes and durations.

The rest of the paper is organized as follows. Our results are all concentrated in Sec. II. We begin in Sec. II A by calculating the right and left tails for the area and perimeter distributions for a single planar BM. We extend these results to N noninteracting BMs in Sec. II B. In Sec. II C, we extend the results to active particles in $d = 2$, uncovering a remarkable sequence of DPTs for the case of multiple RTPs. In Sec. II D we consider higher dimensions, focusing on the volume and surface area distributions for a single BM in $d = 3$. We conclude with a discussion in Sec. III. Several technical details are given in the Appendices.

II. RESULTS

The simplest case is the single BM in $d = 2$. We therefore begin with a full analysis of the two tails for this case,

TABLE I. Behaviors of the left and right tails of the distributions of the area A and perimeter L of the convex hull for different planar stochastic processes of duration T : BM with diffusion coefficient D , N (multiple) BMs, active particles and N active particles, and their extensions to $d > 2$ dimensions (i.e., the volume V and surface area \mathcal{A}). Here $x_1 = 2.4048 \dots$ is the first zero of the Bessel's function $J_0(x)$. The case $N = 2$ is very simply related to the case $N = 1$ and the relation is given by Eq. (17). $\Phi(z)$ is the rate function that describes the distribution of the position of the active particle at long times, see Eq. (28). For the RTP, $\Phi(z)$ is given in Eq. (29). The α_M and β_M are the coefficients of the rate function $\Phi(z)$ for the $N \geq 3$ active particles given by Eq. (41). \tilde{f}_d is the smallest eigenvalue of the minus Laplace operator on the d -dimensional ball of unit radius with absorbing boundary conditions, and \tilde{V}_d and \tilde{A}_d are the volume and surface area, respectively, of the ball of unit radius. Trajectories are open unless stated otherwise.

Dimensions	Types of walk	Observables	Tails	Open, closed	
$d = 2$	BM	Perimeter	Right	Open: $\mathcal{P}(L) \sim e^{-L^2/16DT}$; closed: $\mathcal{P}(L) \sim e^{-L^2/4DT}$ $\mathcal{P}(L) \sim e^{-4\pi^2 x_1^2 DT/L^2}$;	
			Left		
		Area	Right	Open: $\mathcal{P}(A) \sim e^{-\pi A/2DT}$; closed: $\mathcal{P}(A) \sim e^{-\pi A/DT}$ $\mathcal{P}(A) \sim e^{-\pi x_1^2 DT/A}$;	
			Left		
	$N \geq 3$ BMs	Perimeter	Right	$\mathcal{P}(L) \sim e^{-b_N L^2/DT}$, $b_N = 1/36$ $\mathcal{P}(L) \sim e^{-4N\pi^2 x_1^2 DT/L^2}$;	
			Left		
		Area	Right	$\mathcal{P}(A) \sim e^{-c_N A/DT}$, $c_3 = 1/\sqrt{3}$, $c_{N \geq 4} = 1/2$ $\mathcal{P}(A) \sim e^{-N\pi^2 x_1^2 DT/A}$;	
			Left		
	Active particles	Perimeter	Right	$\mathcal{P}(L) \sim e^{-T\Phi(L/2T)}$	
			Area		$\mathcal{P}(A) \sim e^{-T\Phi(\sqrt{2\pi A}/T)}$
$N \geq 3$ active particles		Perimeter	Right	$\mathcal{P}(L) \sim e^{-T \min_M \Phi(\alpha_M L/T)}$, $\alpha_M = (2M \sin \frac{\pi}{M})^{-1}$.	
			Area		$\mathcal{P}(A) \sim e^{-T \min_M \Phi(\beta_M \sqrt{A}/T)}$, $\beta_M = (\frac{M}{2} \sin \frac{2\pi}{M})^{-1/2}$.
$d > 2$	BM	Surface area	Right	$\mathcal{P}(\mathcal{A}) \sim e^{-l_{A,d} \mathcal{A}^{2/(d-1)}/DT}$; $l_{A,3} = \pi/4$ $\mathcal{P}(\mathcal{A}) \sim e^{-\tilde{f}_d DT (\tilde{A}_d/\mathcal{A})^{2/(d-1)}}$	
			left		
			Volume		$\mathcal{P}(V) \sim e^{-l_{V,d} V^{2/d}/DT}$; $l_{V,3} \simeq 5.3$ $\mathcal{P}(V) \sim e^{-\tilde{f}_d DT (\tilde{V}_d/V)^{2/d}}$
			Volume	Right	$\mathcal{P}(V) \sim e^{-l_{V,d} V^{2/d}/DT}$; $l_{V,3} \simeq 5.3$ $\mathcal{P}(V) \sim e^{-\tilde{f}_d DT (\tilde{V}_d/V)^{2/d}}$
				Left	

followed by extensions to multiple and/or active particles. Then we treat the case of a single BM in $d = 3$. The results are summarized in Table I.

A. Single planar Brownian motion

1. Right tail: Large area (A)–large perimeter (L)

Let us begin from the simplest case of a single BM. From the scaling forms (2) and (3) one immediately finds that large perimeters or areas are mathematically equivalent to the short-time and/or weak-noise limit, i.e., $DT \ll A$ or $DT \ll L^2$. The probability is dominated by the most probable path constrained on a given value of the observable of interest (A or L) in a short T limit. In this short T –weak noise limit, the optimal fluctuations method (OFM) [52–64] gives the equation of the optimal path of the motion constrained to a given value of the observable of interest. The path probability of the trajectory $\mathbf{r}(t)$ is given by

$$\mathcal{P}[\mathbf{r}(t)] \sim e^{-s/2D}, \quad (7)$$

where $s[\mathbf{r}(t)]$ is the Wiener action [1]

$$s[\mathbf{r}(t)] = \frac{1}{2} \int_0^T \dot{\mathbf{r}}(t)^2 dt. \quad (8)$$

In the small- DT limit, we apply the saddle-point approximation and thus find that the dominant contribution to $\mathcal{P}(A)$ [$\mathcal{P}(L)$] comes from the minimizer $\mathbf{r}(t)$ (the “optimal trajectory”) of the action constrained on the value of the area (perimeter). The action is minimized by motion with constant speed $|\dot{\mathbf{r}}(t)| = \text{constant}$ with the additional constraints [62–65] (see also Appendix A). The action of the optimal trajectory is

thus given by

$$-\ln \mathcal{P} \simeq s = \frac{\mathcal{L}^2}{4DT}, \quad (9)$$

where \mathcal{L} is the length of the trajectory and \ln denotes the logarithm in the natural basis. The problem thus reduces to minimizing \mathcal{L} constrained on a given value of the observable (area or perimeter).

Let us start by studying the closed case which is a little simpler. Without loss of generality we consider only trajectories that are themselves the boundary of a convex shape, because if this is not the case, then one can always find a shorter trajectory with the same convex hull; see Fig. 1. Under this assumption \mathcal{L} equals the perimeter L of the convex hull.

Consider first the problem of minimizing \mathcal{L} constrained on A . By the argument above, the problem reduces to that of finding a shape of minimal perimeter that encloses a given area (the isoperimetric problem) whose solution has been known for a very long time [66,67]: It is a circle of area A [see Fig. 2(a)]. The area and perimeter of a circle are related via $A = L^2/(4\pi)$. Hence the probability of the right tail behaves as [recalling that $\mathcal{L} = L$ and using Eq. (9)]

$$-\ln \mathcal{P}(A \gg DT) = s = \pi \frac{A}{DT}. \quad (10)$$

Let us now find the minimizer of \mathcal{L} constrained on A for an open BM. We assume that the particle begins at the origin (at time $t = 0$) and, without loss of generality, that it finishes on the x axis at time $t = T$. We additionally assume that the trajectory is contained in the upper half plane $y \geq 0$ (this

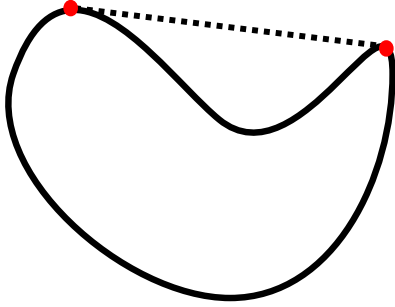


FIG. 1. Schematic diagram of the convex hull of a trajectory of a BM. To minimize the length of the trajectory \mathcal{L} constrained on the convex hull area A or perimeter L , it is more favorable to follow the dotted (straight) line than the solid line, when going between the two points marked in the figure.

assumption will be justified *a posteriori*). As for the closed case, the minimizer cannot have any concave sections. The problem thus reduces to finding the curve of minimal length with the area under the curve constrained to a given value A . This problem is known as Dido’s problem [66,67], which is the extension of the isoperimetric problem. The solution to Dido’s problem is a semicircle of area A [see Fig. 2(b)]. For the semicircle, the length of the trajectory and the area are related via $A = \mathcal{L}^2/2\pi$. Hence, the probability of the right tail for an open BM is given by

$$-\ln \mathcal{P}(A \gg DT) = s = \frac{\pi}{2} \frac{A}{DT}. \quad (11)$$

This optimal trajectory is in agreement with rigorous results from the mathematical literature which were obtained for

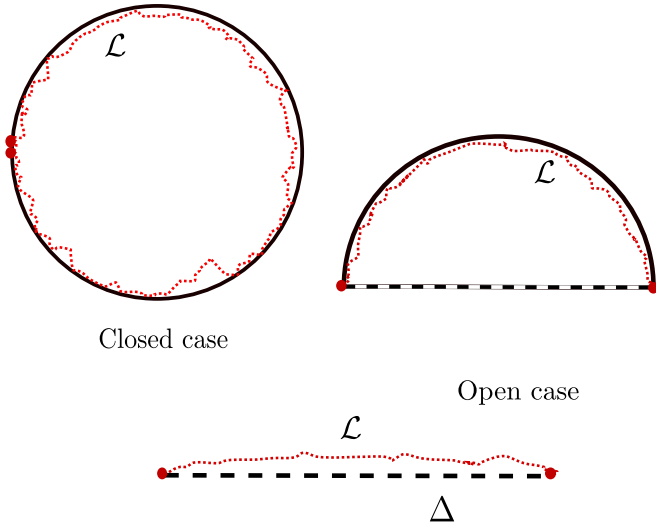


FIG. 2. Solid lines: Trajectories of minimal length \mathcal{L} , corresponding to the right tails of the area and perimeter distributions. For the area distribution, both the open and closed BMs are plotted. Schematic diagrams of the convex hulls formed by BMs of length \mathcal{L} , corresponding to the right tails of the area and perimeter distributions. The dotted lines are a schematic of realistic realizations that attain large but finite area (or perimeter). For the closed case, the hull is a circle for a fixed area A and for the open case, the hull is a half circle for a fixed A and line segment for fixed L .

general open RWs [39]. The result (11) is also in excellent agreement with the numerical data of Ref. [23]; see Fig. 3(a).

Now let us solve the minimization problem of the length \mathcal{L} constrained on the perimeter L . For the closed case, as shown above, $L = \mathcal{L}$ and therefore the minimization problem has a very large degeneracy of solutions (any closed trajectory which is the boundary of a convex shape is a minimizer). For open motion, we assume again that the trajectory stays in the upper half plane (taking the endpoint to be on the x axis) and hence the relation between L and \mathcal{L} is $L = \mathcal{L} + \Delta$, where Δ is the distance between the endpoints of the BM. The minimal \mathcal{L} is obtained when the curve approaches straight line [see Fig. 2(c)], and then one has $\Delta \simeq \mathcal{L}$ so

$$L = \mathcal{L} + \Delta \simeq 2\mathcal{L}. \quad (12)$$

Hence, the right tail of $\mathcal{P}(L)$ behaves as

$$-\ln \mathcal{P}(L \gg \sqrt{DT}) \sim \begin{cases} \frac{L^2}{16DT}, & \text{open,} \\ \frac{L^2}{4DT}, & \text{closed.} \end{cases} \quad (13)$$

The results are in excellent agreement with the numerical data of Ref. [23]; see Fig. 3(b).

2. Left tail: Small area (A)–small perimeter (L)

The small- A (or small- L) limit with constant T is mathematically equivalent, according to Eq. (3), to the long- T limit at constant A (or constant L). In other words, the particle must survive inside the convex hull itself for an unusually long time. The least unlikely way for this to happen is if the convex hull takes the shape of a circle of area A (or perimeter L). We thus argue that $\mathcal{P}(A)$ [or $\mathcal{P}(L)$] is, in the leading order, given by the survival probability inside a circle of area A (or perimeter L). In the leading order, it does not matter whether the BM is open or closed (the difference only affects a short time window in the trajectory, close to $t = T$).

In the long-time limit (large T), the survival probability $S_{\text{prob}}(T|R)$ of a BM inside a d -dimensional ball of radius R is, in the leading order, independent of the initial position within the ball and is dominated by the smallest eigenvalue (in absolute value) of the Laplace operator with absorbing boundary conditions. Therefore, it is given by (see, e.g., [68])

$$-\ln S_{\text{prob}}(T|R) \simeq \begin{cases} \frac{\pi^2}{4R^2} DT, & d = 1, \\ \frac{x_1^2}{R^2} DT, & d = 2, \\ \frac{\pi^2}{R^2} DT, & d = 3, \end{cases} \quad (14)$$

where $x_1 = 2.4048\dots$ is the first positive root of the Bessel function $J_0(z)$.

Using this, we obtain the left tails for the area and perimeter distributions by considering the survival probabilities in a circle of given area (or of given perimeter),

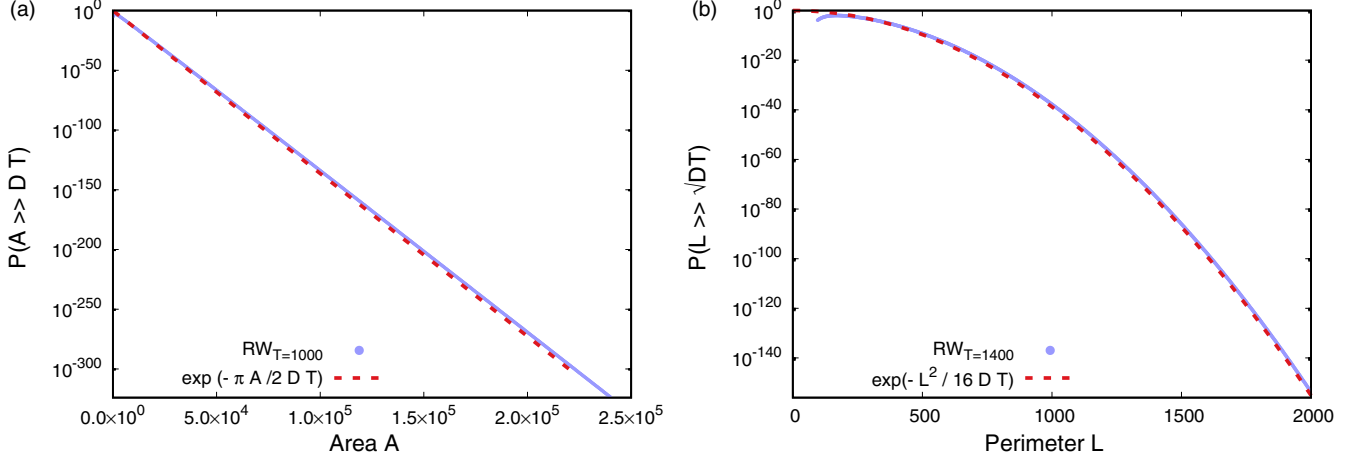


FIG. 3. Right tails of the distributions (in log scale) of the area (a) and perimeter (b) of the convex hull for an open planar BM. The blue solid line depicts the data of $\mathcal{P}(A)$ from [23] and can be seen to be in excellent agreement with the red dashed lines which denote our theoretical predictions. Parameters are $D = 1/2$, and $T = 1000$ (a) and $T = 1400$ (b).

yielding

$$-\ln \mathcal{P}(A \ll DT) \simeq \pi x_1^2 \frac{DT}{A}, \quad (15)$$

$$-\ln \mathcal{P}(L \ll \sqrt{DT}) \simeq 4\pi^2 x_1^2 \frac{DT}{L^2}. \quad (16)$$

These formulas hold both for the open and closed BMs. The scaling behaviors in these results are in agreement with the numerical results in Ref. [23] but the numerical coefficients observed there were different. We believe that this discrepancy is because the numerical simulations use a sufficient number of time steps to observe the continuous BM behavior.

B. Multiple Brownian motions

In this subsection, we consider $N > 1$ noninteracting BMs, beginning from the case $N = 2$ which is particularly simple. In this case, by concatenating the two trajectories we obtain a trajectory that could be considered as that of a single BM of twice the duration. Therefore, the distributions for $N = 2$ are exactly related to those for $N = 1$ via

$$\mathcal{P}(*, T)|_{N=2} = \mathcal{P}(*, 2T)|_{N=1} \quad (17)$$

(where the time dependence is denoted explicitly and $*$ represents area, perimeter, or other such observable). In particular, the distribution tails can thus be obtained immediately from the results reported above for the $N = 1$ case.

Therefore, in the rest of this subsection we will assume that $N \geq 3$. Let us consider first the right tail. Here, following a similar approach to the one we used above for the case $N = 1$, we find that this tail is dominated by the (multiparticle) trajectory that minimizes the sum of the Wiener actions s_{tot} , constrained on a given value of the area or perimeter. The minimum is obtained for trajectories for which each particle's speed is constant, and the sum of the Wiener actions is given by $s_{\text{tot}} = (\sum_{i=1}^N \mathcal{L}_i^2)/4DT$, where \mathcal{L}_i is the length of the trajectory of particle i .

In order to proceed to solve this minimization problem we next assume that the full trajectories of the N particles, except perhaps some of the endpoints, are all in the interior of the

convex hull (this assumption will be justified *a posteriori*). Thus only the endpoints of these trajectories are important, and the optimal trajectories must be straight lines. This simplifies the minimization problem considerably, because now we are just minimizing a function of the endpoints (and not a functional of the entire trajectories).

For any $3 \leq M \leq N$ there exists a solution to this minimization problem for which M of the particles travel the same distance $\mathcal{L}_i = \mathcal{L}$ in straight lines, and leaving the origin at equally spaced angles, while the remaining $N - M$ particles remain near the origin. Thus, the convex hull that is formed by these trajectories is a regular polygon of M sides (see Fig. 4 for an example with $N = 6$ and $M = 5$ in shaded region). The action $s_M = s_{\text{tot}}$ for each of these solutions can be expressed as

$$s_M(L) = \tilde{b}_M \frac{L^2}{DT}, \quad (18)$$

$$s_M(A) = \tilde{c}_M \frac{A}{DT}. \quad (19)$$

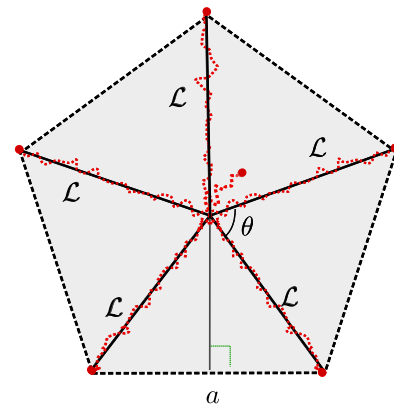


FIG. 4. Schematic diagram of the convex hull formed by N BMs of length \mathcal{L} . Here $N = 6$, $M = 5$, and $\theta = \frac{2\pi}{M}$ is the angle between two BMs participating in the solution. As explained in the text, the solutions with $M = 3$ and $M = 4$ are the optimal solution for perimeter and area, respectively.

TABLE II. Coefficients of the action $s_M(L)$ and $s_M(A)$, respectively, given in Eq. (18) for N noninteracting BMs. The minimum is obtained at $M = 3$ ($M = 4$) for the perimeter (area) case.

M	$\tilde{b}_M = (16M \sin^2 \frac{\pi}{M})^{-1}$	$\tilde{c}_M = (2 \sin \frac{2\pi}{M})^{-1}$
3	$1/36 = 0.027 \dots$	$1/\sqrt{3} = 0.57 \dots$
4	$1/32 = 0.031 \dots$	$1/2 = 0.5$
5	$(5 + \sqrt{5})/200 = 0.036 \dots$	$\sqrt{2/\sqrt{5} + 5} = 0.525 \dots$
6	$1/24 = 0.041 \dots$	$1/\sqrt{3} = 0.577 \dots$
7	$0.047 \dots$	$0.639 \dots$
$M \gg 1$	$\simeq M/16\pi^2$	$\simeq M^2/4\pi$

The coefficients \tilde{b}_M and \tilde{c}_M are of geometric origin: They are calculated from the relation between \mathcal{L} and L or A , respectively, for a regular M -sided polygon. For an M -sided polygon (for example Fig. 4 for $M = 5$), the perimeter is $L = Ma$, where $a = 2\mathcal{L} \sin \theta$ is the length of each side of the polygon, which implies $L = (2M \sin \frac{\pi}{M})\mathcal{L}$. Similarly, the area is given by $A = (M \sin \frac{\pi}{M} \cos \frac{\pi}{M})\mathcal{L}^2$. Finally, using that the total action is $s_M = M\mathcal{L}^2/4DT$, we obtain the coefficients

$$\tilde{b}_M = \frac{1}{16M \sin^2 \frac{\pi}{M}}, \quad \tilde{c}_M = \frac{1}{2 \sin \frac{2\pi}{M}}. \quad (20)$$

These solutions all represent *local* minima of the action s_M , and in order to find the *global* minimum, we must now perform an additional minimization over $M = 3, 4, \dots, N$. This amounts to minimizing the coefficients \tilde{b}_M and \tilde{c}_M over M for the perimeter and area, respectively. These coefficients are tabulated in Table II. We find, and show explicitly in Appendix B 1, that $M = 3$ ($M = 4$) is minimal (over all values $M = 3, 4, \dots$) for the perimeter (area) case. Therefore the optimal convex hull shape is an equilateral triangle whose center is the origin for the perimeter case and for the area case with $N = 3$ and a square centered at the origin for the area case with $N \geq 4$. So the probability is now expressed for any $N \geq 3$ as (see Table I)

$$\mathcal{P}(L) \sim e^{-b_N L^2/DT}, \quad b_N = \min_{3 \leq M \leq N} \tilde{b}_M = \tilde{b}_3 = \frac{1}{36},$$

$$\mathcal{P}(A) \sim e^{-c_N A/DT}, \quad (21)$$

$$c_N = \min_{3 \leq M \leq N} \tilde{c}_M = \begin{cases} \tilde{c}_3 = \frac{1}{\sqrt{3}}, & N = 3, \\ \tilde{c}_4 = \frac{1}{2}, & N \geq 4. \end{cases} \quad (22)$$

Thus, rather remarkably, the right tail of the perimeter (area) distribution becomes, in the leading order, independent of N for $N \geq 3$ ($N \geq 4$). These theoretical predictions exhibit excellent agreement with the numerical observations from Ref. [24]; see Appendix B 2.

The left tails of the distributions of A and L for N noninteracting particles behave very similarly to the single particle case. They are dominated by the survival probability of N particles inside a circle of appropriate area (or perimeter). Since the particles are noninteracting, the latter probability is simply given by that of a single particle, raised to the power N . Using the middle line of (14) together with the relations

between the radius of a circle and its perimeter and area, one finds

$$\mathcal{P}(A) \sim e^{-\pi x_1^2 NDT/A}, \quad (23)$$

$$\mathcal{P}(L) \sim e^{-4\pi^2 x_1^2 NDT/L^2}. \quad (24)$$

C. Active particles

As described above, for a broad class of models of active models, the long-time typical behavior is diffusive, with an effective diffusion coefficient that can be found (see examples above for the cases of the RTP and ABP). Thus, we expect that both the typical fluctuations and the near tails of the area and perimeter distributions behave, at long times $T \gg \tau$ (where, to remind the reader, τ is the correlation time of the active noise), and coincide with those of BM. The signatures of activity are expected to be found in the far tails of the distribution. In this subsection, we will focus on the behavior in the right tail. The left tail probabilities are still expected to be given by the long-time survival probabilities inside circles of appropriate sizes. We do not attempt to calculate these survival probabilities in the current work; see, however, the recent Ref. [69] in which this was achieved for the ABP (see also the related work [70] where the RTP in $d = 1$ was studied).

1. Coarse graining

For active particles, in the long-time limit (where T is much larger than the correlation time τ of the noise Σ), one can coarse grain the noise $\Sigma(t)$ that is coarse grained by averaging it over intermediate timescales $\tau \ll \Delta t \ll T$ [71–79],

$$\bar{\Sigma}(t) = \frac{1}{\Delta t} \int_t^{t+\Delta t} \Sigma(t') dt'. \quad (25)$$

The probability of a coarse-grained noise history $\bar{\Sigma}(t)$ is given (in the leading order) by the “temporal additivity principle,”

$$\mathcal{P}[\bar{\Sigma}(t)] \sim \exp\{-s[\bar{\Sigma}(t)]\}, \quad (26)$$

where the action $s[\bar{\Sigma}(t)]$ is now given by

$$s[\bar{\Sigma}(t)] = \int_0^T \Phi[\bar{\Sigma}(t)] dt. \quad (27)$$

Here we assume that the long-time position distribution $\mathcal{P}(x, y, t)$ of the particle satisfies an large deviation principle (LDP) [38,41] with a rate function $\Phi(z)$, i.e., that

$$\mathcal{P}(x, y, t) \sim e^{-t\Phi(x/t, y/t)}. \quad (28)$$

$\Phi(z)$ is known for several standard models of active particles including RTP and ABP. For the RTP [Eq. (6)] it was calculated exactly to be [51,78,80]

$$\Phi(v) = 2\gamma\phi(v/v_0), \quad \phi(z) = 1 - \sqrt{1 - z^2}. \quad (29)$$

For ABP [see Eq. (5)], the Φ was found exactly in Refs. [81–83] in terms of the smallest eigenvalue that gives periodic solutions to the Mathieu equation. In fact, the LDP (28) holds for many types of random walks in discrete time and/or space, where the rate function can be found from Cramér’s theorem, see, e.g., Ref. [41].

The coarse-grained Langevin equation, obtained by replacing $\Sigma(t)$ by $\bar{\Sigma}$ in Eq. (4), is

$$\dot{\mathbf{r}}(t) = \bar{\Sigma}(t). \quad (30)$$

For rotationally invariant statistics of the noise $\Sigma(t)$, the $\Phi[\mathbf{z}]$ is also rotationally symmetric, $\Phi[\mathbf{z}] = \Phi[z]$.

As in the case of BM, the minimizer of (27) is obtained for trajectories for which the argument of Φ is of constant modulus which simply equals the speed \mathcal{L}/T (see Appendix A). Therefore, we simply get

$$s = T\Phi(\mathcal{L}/T), \quad (31)$$

where \mathcal{L} is the length of the trajectory. Thus, we find that here, too, the problem boils down to minimizing \mathcal{L} under the constraints.

2. Right tail for a single active particle

Using Eq. (31), we find that the right tails of the area and perimeter distributions can be calculated by replacing $\mathcal{L}^2/4DT$ in Eq. (9) by $T\Phi(\mathcal{L}/T)$. Thus, the right tails of the perimeter and area distributions for the closed and open cases are given by

$$\ln \mathcal{P}(L) \simeq \begin{cases} -\gamma T \Phi(L/T), & \text{closed,} \\ -\gamma T \Phi(L/2T), & \text{open,} \end{cases} \quad (32)$$

$$\ln \mathcal{P}(A) \simeq \begin{cases} -\gamma T \Phi(\sqrt{4\pi A}/T), & \text{closed,} \\ -\gamma T \Phi(\sqrt{\pi A}/T), & \text{open.} \end{cases} \quad (33)$$

To give an explicit, concrete example, let us consider the RTP. For the RTP, using Eq. (29) the right distribution tails for the open case are given by

$$\ln \mathcal{P}(L) \simeq -\gamma \left(T - \sqrt{T^2 - \frac{L^2}{v_0^2}} \right); \quad L \gg \sqrt{D_{\text{eff}} T}, \quad (34)$$

$$\ln \mathcal{P}(A) \simeq -\gamma \left(T - \sqrt{T^2 - \frac{4\pi A}{v_0^2}} \right); \quad A \gg D_{\text{eff}} T, \quad (35)$$

where D_{eff} is the effective diffusion coefficient. Figure 5 shows the right tail of the perimeter for $T = 512$, which fits well with the experimental data from Ref. [28]. For small $|z| \ll 1$, the $\Phi(z)$ can be approximated as a parabola,

$$\Phi(z) \simeq \frac{z^2}{2}, \quad (36)$$

which corresponds to passive limit and the action in Eq. (27) reduces to the Wiener action (8) [1], which is the BM limit. As a result, the near right tail of the distribution, $\sqrt{D_{\text{eff}} T} \ll L \ll v_0 T$, coincides with that of the BM result, see Fig. 5.

3. Dynamical phase transitions for multiple active particles

Let us now analyze the case of $N > 1$ active particles. We first consider the case $N = 2$. At $T \gg \tau$, the argument used above for BMs, to relate the cases $N = 2$ and $N = 1$, still holds (but only approximately). Thus, Eq. (17) still approximately holds at long times both in the typical-fluctuations and large-deviation regimes.

Let us now analyze the case $N \geq 3$, focusing on the right tail. The analysis is similar to the case of $N \geq 3$ BMs studied above (see Sec. II B). One must minimize the sum of

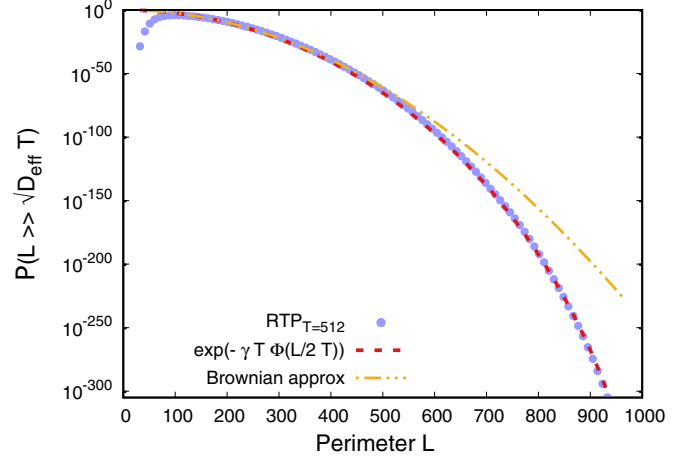


FIG. 5. Right tail of the distribution $\mathcal{P}(L)$ of perimeter L of the convex hull for a RTP for walk length $T = 512$ and $\gamma = v_0 = 1$. The blue circles depict the numerical data from Ref. [28] and the red dashed lines denote our theoretical prediction. The yellow dot-dashed line denotes the corresponding BM result, obtained by applying the parabolic Brownian approximation (36) of the rate function $\Phi(z)$. The Brownian approximation can be seen to correctly describe the near tail of the distribution, but it breaks down in the far tail.

the coarse-grained actions $s_{\text{tot}} = T \sum_{i=1}^N \Phi(\mathcal{L}_i/T)$. We again assume that the trajectories of the N active particles reside within the interior of the convex hull, except for some of the trajectories' endpoints. Thus, the optimal paths are all straight lines, and the problem reduces to that of minimizing s_{tot} with respect to the endpoints of the trajectories. Again we find that for each $3 \leq M \leq N$ there exists a solution in which M particles exit the origin at equally spaced angles, and each travel a distance of $\mathcal{L}_i = \mathcal{L}$, while the remaining $N - M$ particles stay near the origin, creating a convex hull whose shape is a regular polygon with M sides, see Fig. 4. However, the actions $s_M = s_{\text{tot}}$ of these solutions, $s_M = MT\Phi(\mathcal{L}/T)$, are different to those of the BMs' case. As a result, the optimal value of M may, too, be different, and as we show below, it can in fact change within the tail, leading to DPTs which are generically of the first order.

Therefore, the right tails of the perimeter and area distributions are determined by the solution with optimal M , i.e., that minimizes s_M ,

$$\mathcal{P}(L) \sim e^{-T\Psi_N(L/T)}, \quad (37)$$

$$\mathcal{P}(A) \sim e^{-T\Psi_N(\sqrt{A}/T)}, \quad (38)$$

where the large-deviation functions Ψ_N are related to the s_M 's above via

$$\Psi_N(L/T) = \min_{3 \leq M \leq N} M\Phi(\alpha_M L/T), \quad (39)$$

$$\Psi_N(\sqrt{A}/T) = \min_{3 \leq M \leq N} M\Phi(\beta_M \sqrt{A}/T). \quad (40)$$

Here the coefficients α_M and β_M are calculated from the geometric relation between \mathcal{L} and L or A , respectively, similarly to the multiple BMs in Fig. 4 in Sec. II B, i.e., $L = (2M \sin \frac{\pi}{M})\mathcal{L}$

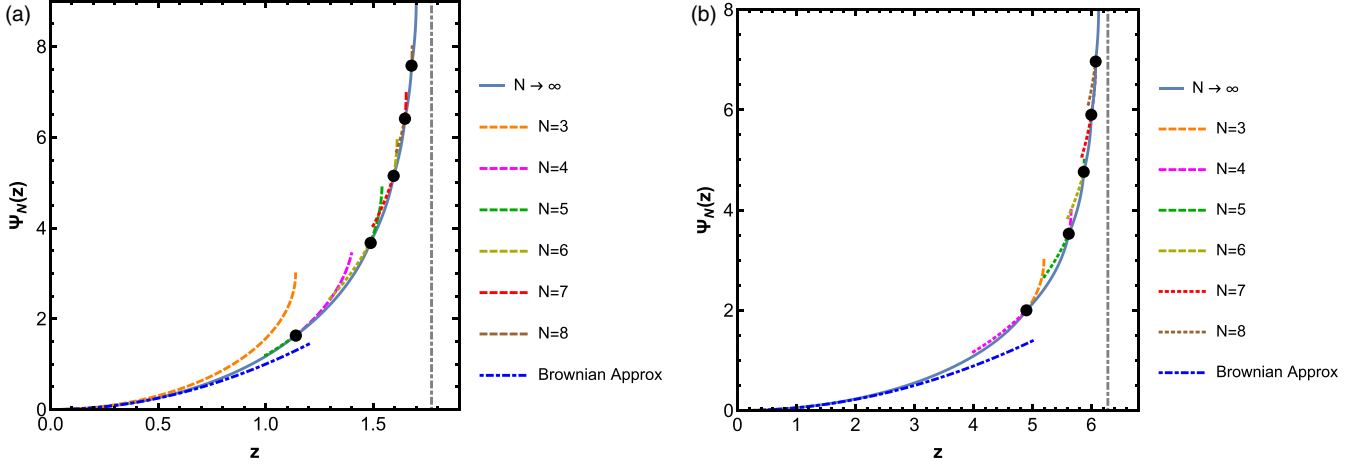


FIG. 6. The rate function $\psi_N(z)$ that describes the right distribution tail for (a) area A and (b) perimeter L for N RTPs. The solid blue line depicts $\psi_{N \rightarrow \infty}$ while the dashed lines correspond to ψ_N for finite values of $N = 3, 4, \dots$ (from bottom to top). The dotted lines correspond to $\tilde{\psi}_M$ in regions where they are not optimal for any value of N (again increasing with M from bottom to top). The circles denote the critical points z_M at which the optimal solution changes from one local minima (M) to another local minima ($M + 1$), signaling a first-order DPT. The blue parabolic dot-dashed lines correspond to the BM approximations [for $N \geq 4$ in (a)] and are seen to give the correct asymptotic behavior at $z \ll 1$, describing the near right tail of the distribution. The vertical, gray dot-dashed lines denote the value that the area or perimeter cannot possibly exceed for any N , corresponding to a convex hull which is a circle of radius $v_0 T$.

and $A = (M \sin \frac{\pi}{M} \cos \frac{\pi}{M}) \mathcal{L}^2$. Hence the α_M and β_M are related to \tilde{b}_M and \tilde{c}_M as:

$$\alpha_M = 4\sqrt{M\tilde{b}_M} = \frac{1}{2M \sin \frac{\pi}{M}}, \quad (41)$$

$$\beta_M = 2\sqrt{\tilde{c}_M/M} = \frac{1}{\sqrt{M \sin \frac{\pi}{M} \cos \frac{\pi}{M}}}. \quad (42)$$

Let us now give explicit results for the particular case of multiple RTPs. Here the rate functions are conveniently written as

$$\Psi_N(v) = 2\gamma \psi_N(v/v_0), \quad (43)$$

where the ψ_N 's are dimensionless and are given by

$$\psi_N(z) = \min_{3 \leq M \leq N} \tilde{\psi}_M(z) \quad (44)$$

and $\tilde{\psi}_M$ is related to the dimensionless rate function ϕ in Eq. (29) that describes the position distribution of a single particle,

$$\begin{aligned} \tilde{\psi}_M(z) &= M\phi(a_M z) = M(1 - \sqrt{1 - a_M^2 z^2}) \\ &= \begin{cases} M \left[1 - \sqrt{1 - \frac{z^2}{4M^2 \sin^2(\pi/M)}} \right] & \text{(perimeter)} \\ M \left[1 - \sqrt{1 - \frac{z^2}{M \sin(\pi/M) \cos(\pi/M)}} \right] & \text{(area)} \end{cases}, \end{aligned} \quad (45)$$

where $a_M = \alpha_M, \beta_M$ for perimeter and area, respectively.

In the near right tails, the value of M that dominates is the same as for the case of BMs. For $T \gg \tau$, the right tail of the N active particles behave like the N noninteracting BMs where the action for $M = 3$ in case of perimeter and $M = 4$ in case of area dominates. Further into the right tail (for sufficiently large N), however, activity dominates and the $M = 4$ (for perimeter) and $M = 5$ (for area) become the optimal solution.

This leads to singularity in the rate function $\psi_N(z)$ which we interpret as a DPT, at a critical value of z , shown by the solid black circle in Fig. 6. Further into the tail further successive DPTs occur from $M = i$ to $M = i + 1$ for $i = 3, \dots, M - 1$ in case of perimeter and for $i = 4, \dots, M - 1$ in case of area. So the right tail of the distribution exhibits $N - 3$ and $N - 4$ DPTs for perimeter and area, respectively. As the transitions occur when the graphs of two $\tilde{\psi}_M$'s cross each other, this transition is of first order in nature, i.e., the first derivative of ψ_N jumps at the critical point.

The coordinates of the critical points can be calculated by requiring $\tilde{\psi}_M(z) = \tilde{\psi}_{M+1}(z)$, which, using Eq. (45), gives

$$M(1 - \sqrt{1 - a_M^2 z^2}) = (M + 1)(1 - \sqrt{1 - a_{M+1}^2 z^2}). \quad (46)$$

The solution to this equation yields the critical points $z = z_M$, which are given by

$$z_M = -\frac{2\sqrt{M(M+1)}\sqrt{a_{M+1}^2(M+1) - a_M^2 M}}{a_M^2 M^2 - a_{M+1}^2 (M+1)^2}. \quad (47)$$

The first few critical points are at

$$z_3 = 2\sqrt{6} = 4.898\dots, \quad z_4 = 2\sqrt{8\sqrt{5} - 10} = 5.617\dots, \quad (48)$$

for the perimeter, and at

$$z_4 = 1.141\dots, \quad z_5 = 1.489\dots, \quad (49)$$

for the area, respectively. The corresponding critical values of L and A are given by $L = z_M v_0 T$ and $A = (z_M v_0 T)^2$.

More generally, it is reasonable to expect that similar DPTs may occur in many models of active particle, and not just in the particular case of the RTP as shown here. In particular, if the particle's speed is bounded, e.g., for the ABP, then we

conjecture that the qualitative picture is very similar to that of the RTP.

D. $d > 2$

Let us now consider the convex hull in higher dimensions ($d > 2$). The arguments above can be extended straightforwardly to study the volume (V) and surface area (\mathcal{A}) distributions of the convex hull in higher dimensions $d > 2$. For instance, for a single BM, this leads to the following behaviors in the tails:

$$\mathcal{P}(V) \sim \begin{cases} e^{-l_{V,d}V^{2/d}/DT}, & V \gg (DT)^{d/2} \\ e^{-\tilde{f}_dDT(\tilde{V}_d/V)^{2/d}}, & V \ll (DT)^{d/2}, \end{cases} \quad (50)$$

$$\mathcal{P}(\mathcal{A}) \sim \begin{cases} e^{-l_{\mathcal{A},d}\mathcal{A}^{2/(d-1)}/DT}, & \mathcal{A} \gg (DT)^{(d-1)/2} \\ e^{-\tilde{f}_dDT(\tilde{\mathcal{A}}_d/\mathcal{A})^{2/(d-1)}}, & \mathcal{A} \ll (DT)^{(d-1)/2}. \end{cases} \quad (51)$$

Here \tilde{f}_d is the smallest eigenvalue of the minus Laplace operator on the d -dimensional ball of unit radius with absorbing boundary conditions; \tilde{V}_d and $\tilde{\mathcal{A}}_d$ are the volume and surface area, respectively, of the ball of unit radius (see, e.g., Ref. [68]); and $l_{V,d}$ ($l_{\mathcal{A},d}$) is a coefficient calculated from the geometric relations between the \mathcal{L} and V (\mathcal{A}) in $d > 2$ dimensions. The coefficients for the right tails are found by minimizing \mathcal{L} constrained on V (or \mathcal{A}). This minimization problem appears to become more difficult as d is increased. The scaling behaviors (50) were conjectured and numerically observed in Ref. [25].

For $d = 3$ we conjecture that the curve of minimal length constrained on a convex-hull surface area \mathcal{A} is in fact confined to a plane (which, without loss of generality, can be taken to be the xz plane) and follows the edge a semicircle of area $\mathcal{A}/2$. The convex hull is thus a semicircle shaped slice of infinitesimal width, so its surface area is \mathcal{A} . The reasoning behind this conjecture is as follows. The curve is optimal with respect to deformations within the xz plane; this follows from the solution to the $d = 2$ problem conditioned on the area \mathcal{A} (see above). On the other hand, both the curve's length \mathcal{L} and the convex hull's surface area \mathcal{A} are mirror symmetric with respect to deformations of the curve in the y direction (perpendicular to the curve). It follows that for the semicircular curve, the variation of \mathcal{L} constrained on \mathcal{A} indeed vanishes, and therefore this curve is a natural candidate for the (global) constrained minimizer. For this curve, \mathcal{A} and \mathcal{L} are related via $\mathcal{A}/\mathcal{L}^2 = \pi$ and using this in Eq. (9) leads to a coefficient of $l_{\mathcal{A},d=3} = \pi/4$.

Very strong evidence in favor of our conjecture is that this coefficient is in agreement with the numerically observed coefficient from Ref. [25]; see Ref. [84]. To further verify our conjecture, we numerically minimized \mathcal{L} constrained on \mathcal{A} using a gradient descent algorithm and found that the shortest curve conditioned on a given surface area indeed appears to be a semicircle (see Fig. 7). To summarize, the scaling behaviors of the tails of the surface-area distribution in $d = 3$ are given by

$$\mathcal{P}(\mathcal{A}) \sim \begin{cases} e^{-\pi\mathcal{A}/4DT}, & \mathcal{A} \gg DT \\ e^{-4\pi^3DT/\mathcal{A}}, & \mathcal{A} \ll DT, \end{cases} \quad (52)$$

where we also plugged in the values of \tilde{f}_3 and $\tilde{\mathcal{A}}_3$.

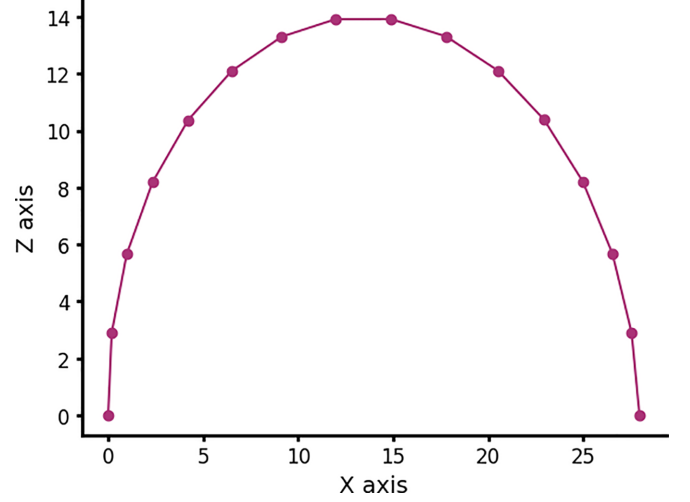


FIG. 7. The shortest curve in the three-dimensional space whose convex hull has a given surface area, obtained numerically using a gradient-descent algorithm. The figure shows the projection of the trajectory onto the xz plane. The y components of all the points are very small on the scale of the figure.

For the volume (in $d = 3$) we were not able to obtain an analytical result for the coefficient $l_{V,3}$, but it was found numerically to be $\simeq 5.3$ in Ref. [25] (see Ref. [84]). The tail behaviors of the volume distribution are thus given by

$$\mathcal{P}(V) \sim \begin{cases} e^{-5.3V^{2/3}/DT}, & V \gg (DT)^{3/2} \\ e^{-(4\pi^2/3)^{2/3}DT/V^{2/3}}, & V \ll (DT)^{3/2}, \end{cases} \quad (53)$$

where we plugged in the values of \tilde{f}_3 and \tilde{V}_3 .

One can extend the analysis to $N > 1$ particles and/or to active particles, as we did above for the case $d = 2$, but we will not do so here. We do expect, however, that some of the qualitative features that we found in $d = 2$ will hold in arbitrary d . In particular, we expect that (i) the relations found above between $N = 2$ and $N = 1$ hold in arbitrary d . (ii) In the leading order, the right tails of $\mathcal{P}(V)$ and $\mathcal{P}(\mathcal{A})$ become independent of N for sufficiently large N . (iii) For N active particles, the right tails of $\mathcal{P}(V)$ and $\mathcal{P}(\mathcal{A})$ will be described by rate functions that are simply related to the rate function Φ , and for sufficiently large N , first-order DPTs will occur.

III. DISCUSSION

We analytically studied the tails of the distributions of area \mathcal{A} and perimeter L of convex hulls formed by the motion of active or passive particles in the plane, and analogous quantities in $d > 2$. We achieved this by identifying the scenario(s) that dominate the contribution to the probabilities of the rare events in question. Our findings are summarized in Table I.

In the left tails, the scenario is that of long-time survival of the particles inside a circle of appropriate size. In the right tails, the OFM is valid, i.e., the probabilities are dominated by the most likely trajectory (or coarse-grained trajectory in the case of active particles) constrained on the observable. Remarkably, we found that the right tails of $\mathcal{P}(L)$ and $\mathcal{P}(\mathcal{A})$ for N BMs become, in the leading order, independent of N at $N \geq 3$ and $N \geq 4$, respectively. This is because the optimal

path involves significant motion of only three (four) of the particles for the perimeter (area) distribution.

For a single arbitrary rotational-invariant active particle, we calculated the exact LDFs that describe the right tails of the distributions of the area and perimeter at times T that are much longer than the microscopic characteristic timescale of the particle. Remarkably, we found that these LDFs are simply related to the rate function Φ that describes the long-time position distribution of the active particle; see Eqs. (32) and (33). We then extended these results to N noninteracting active particles; see Eqs. (39) and (40). We found that, depending on Φ , there may be DPTs in the right tails, signaling a sudden change in the behavior of the system as critical values of L (or A) are crossed. We illustrated this by calculating the LDFs explicitly for the case of the RTPs, where we found that for $N > 3$ ($N > 4$), the right tail of the perimeter (area) distribution exhibits $N - 3$ ($N - 4$) such DPTs, which are all of the first order. Note that although we stated our results in the context of active particles, they are more general and cover a broad class of models (e.g., RWs that are discrete in time and/or space) for which the large-deviation principle (28) holds (with a rotationally invariant Φ).

Finally, we have considered the distribution of surface area and hypervolume of the convex hull for a BM in $d > 2$ dimensions, with special emphasis on the case $d = 3$. We calculated the left tails: They are again given by the survival probability inside a hypersphere of appropriate size. We were able to obtain the scaling behavior in the right tails up to a numerical constant, which is found by solving a minimization problem. This problem appears to be difficult to solve analytically in general, but we were able to obtain its solution for the surface area case in $d = 3$. In other cases, one can solve the problem numerically.

In many of the cases that we studied here, we were able to compare our theoretical predictions with existing numerical data, showing excellent agreement in the right tails in all cases. We hope that this work will stimulate additional numerical investigations (in particular, in the left tails where we believe that more extensive numerical work is needed in order to observe convergence to the theoretical results).

Several interesting future directions of research remain. It would be interesting to extend our results to nonrotationally invariant active particles [40] and/or to the case in which there is an external drift acting on the particle [22]. Another interesting future direction is to analytically study the tail distributions for self-avoiding RWs, which were investigated numerically in Refs. [26,27]. Finally, it would be interesting to study the left tails for active particles (by analyzing their long-time survival probabilities in circles of given sizes) and also to study the $N \gg 1$ limiting behaviors of the distributions [24] for both active and passive particles.

ACKNOWLEDGMENTS

We thank Baruch Meerson, Grégory Schehr, and Satya Majumdar for useful discussions. We are very grateful to Hendrik Schawe, Timo Dewenter, and Alexander Hartmann for sending numerical data of Refs. [23,24,28]. We acknowledge support from the Israel Science Foundation (ISF) through Grant No. 2651/23. S.M. thanks the LPTMS for hospitality.

APPENDIX A: MINIMAL-ACTION TRAJECTORIES HAVE CONSTANT SPEED

In this Appendix we show that the optimal paths have constant speed. We will show it for active particles with rate function Φ and treat BM as a particular case in which $\Phi(z) \propto z^2$. For concreteness, we treat the case $d = 3$, but the proof immediately extend to any dimension.

The action of a trajectory of an active particle in $d = 3$, corresponding to the coarse-grained equation (30), is

$$s[\vec{r}(t)] = \int_0^T \Phi(\sqrt{\dot{x}^2 + \dot{y}^2 + \dot{z}^2}) dt. \quad (\text{A1})$$

Consider a given curve in the xyz space, represented in parametric form by $(x_0(s), y_0(s), z_0(s))$ with $0 \leq s \leq 1$. Then all time-dependent trajectories that follow this curve can be written in the form

$$(x(t), y(t), z(t)) = (x_0[f(t)], y_0[f(t)], z_0[f(t)]) \quad (\text{A2})$$

for some monotonically increasing function $f: [0, 1] \rightarrow [0, T]$ that satisfies $f(0) = 0$, $f(1) = T$.

Restricting ourselves to trajectories that follow such a curve, we rewrite the action (A1) as a functional of the function f . By using the chain rule in (A1) one obtains

$$s[\vec{r}(t)] = \int_0^T \Phi(\dot{f} \sqrt{x_0'^2 + y_0'^2 + z_0'^2}) dt, \quad (\text{A3})$$

where we use the shorthand notation $x_0' \equiv x_0'[f(t)]$ and similarly for y_0' and z_0' . The Lagrangian $L = \Phi(\dot{f} \sqrt{x_0'^2 + y_0'^2 + z_0'^2})$ does not explicitly depend on time t , so the Hamiltonian H is conserved. In order to calculate H , we calculate the conjugate momentum of f ,

$$p = \frac{\partial L}{\partial \dot{f}} = \Phi'(\dot{f} \sqrt{x_0'^2 + y_0'^2 + z_0'^2}) \sqrt{x_0'^2 + y_0'^2 + z_0'^2}, \quad (\text{A4})$$

which yields

$$\begin{aligned} H &= \dot{f} p - L \\ &= \dot{f} \sqrt{x_0'^2 + y_0'^2 + z_0'^2} \Phi'(\dot{f} \sqrt{x_0'^2 + y_0'^2 + z_0'^2}) \\ &\quad - \Phi(\dot{f} \sqrt{x_0'^2 + y_0'^2 + z_0'^2}) \\ &= E = \text{constant in time.} \end{aligned} \quad (\text{A5})$$

So H is conserved in time. One can rewrite H in Eq. (A5) as a function only of the speed $v = \sqrt{\dot{x}^2 + \dot{y}^2 + \dot{z}^2}$, as $H = v \Phi'(v) - \Phi(v)$. It follows that the speed along the trajectory is constant in time and is given by

$$\sqrt{\dot{x}^2 + \dot{y}^2 + \dot{z}^2} = \text{const} = \mathcal{L}/T, \quad (\text{A6})$$

where \mathcal{L} is the length of the curve (x_0, y_0, z_0) . Plugging this back into Eq. (A1) one finds that the action evaluated along the optimal trajectory [constrained on a given curve (x_0, y_0, z_0)] is given by

$$s[\vec{r}(t)] = \int_0^T \Phi\left(\frac{\mathcal{L}}{T}\right) dt = T \Phi\left(\frac{\mathcal{L}}{T}\right). \quad (\text{A7})$$

The expression (A7) is an increasing function of \mathcal{L} , and therefore its minimization with respect to curves (x_0, y_0, z_0) (under various constraints such as convex-hull perimeter or

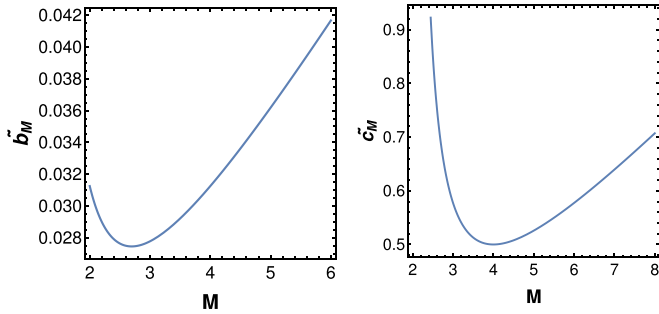


FIG. 8. Coefficients \tilde{b}_M and \tilde{c}_M as a function of M . The $M = 3$ and $M = 4$ are optimal solutions for perimeter and area, respectively, i.e., they minimize the functions \tilde{b}_M and \tilde{c}_M over integer values $M \geq 3$.

area) boils down to the minimization of the length of the curve (under the constraints), as explained in the main text.

It is straightforward to extend this argument to arbitrary dimension $d > 1$.

APPENDIX B: MULTIPLE BROWNIAN MOTIONS

1. Showing that $M = 3, 4$ are optimal

In this section, we explicitly show that $M = 3$ and $M = 4$ solutions are optimal for multiple BMs for perimeter and area, respectively, as stated in Sec. II B. As tabulated in Table II, the coefficients \tilde{b}_M and \tilde{c}_M of the action

$$\tilde{b}_M = \frac{1}{16M \sin^2 \frac{\pi}{M}}, \quad \tilde{c}_M = \frac{1}{2 \sin \frac{2\pi}{M}}, \quad (\text{B1})$$

obtain their minima at $M = 3$ and $M = 4$, respectively.

It is fairly easy to see that \tilde{c}_M attains its minimum (for $M \geq 2$) at $M = 4$. This is because for $M = 4$, the sine function in

the denominator attains its maximal value 1. Let us now show that \tilde{b}_M attains its minimum (for integer $M > 2$) at $M = 3$. For this, let us first minimize \tilde{b}_M for real values of $M > 2$ or, equivalently, maximize $g(M) = 1/\tilde{b}_M = 16M \sin^2 \frac{\pi}{M}$. The requirement $g'(M) = 0$ yields the transcendental equation

$$\tan \frac{\pi}{M} = \frac{2\pi}{M}. \quad (\text{B2})$$

This equation has a unique (real) solution, $M = 2.695 \dots$, which corresponds to the global minimum of \tilde{b}_M for real $M > 2$. Therefore, the minimum of \tilde{b}_M for integer $M > 2$ is at $M = 3$. \tilde{b}_M and \tilde{c}_M are plotted, as functions of real M , in Fig. 8.

2. Comparison with numerics

In this subsection, we compare our expressions (21) and (22) for the right tails of the convex-hull perimeter and area distributions for N noninteracting BMs with the numerical data taken from Ref. [24] (see Fig. 9). We used *webplotdigital* software to collect the data from the Figs. 11 and 12 of Ref. [24]. The numerical data provided in Ref. [24] is for RW in discrete time and standard Gaussian step distribution. The parameters that they chose were such that the time step was unity, corresponding to a diffusion coefficient $D = 1/2$, and they used $T = 50$.

For the perimeter distribution, we observe excellent agreement with our prediction for the coefficient $b_N = \frac{1}{36}$, for all $N \geq 3$ [see Fig. 9(a)]. Indeed, we find that the numerical data for $N = 3$ and $N = 4$ both fall on the same theoretical curve. For the area distribution, we find that the numerical results are in excellent agreement with our predictions for the coefficients, $c_3 = 1/\sqrt{3}$ and $c_N = 1/2$ for all $N \geq 4$. Indeed, we find that the numerical results for $N = 4$ and $N = 6$ both fall on the same theoretical curve [see Fig. 9(b)].

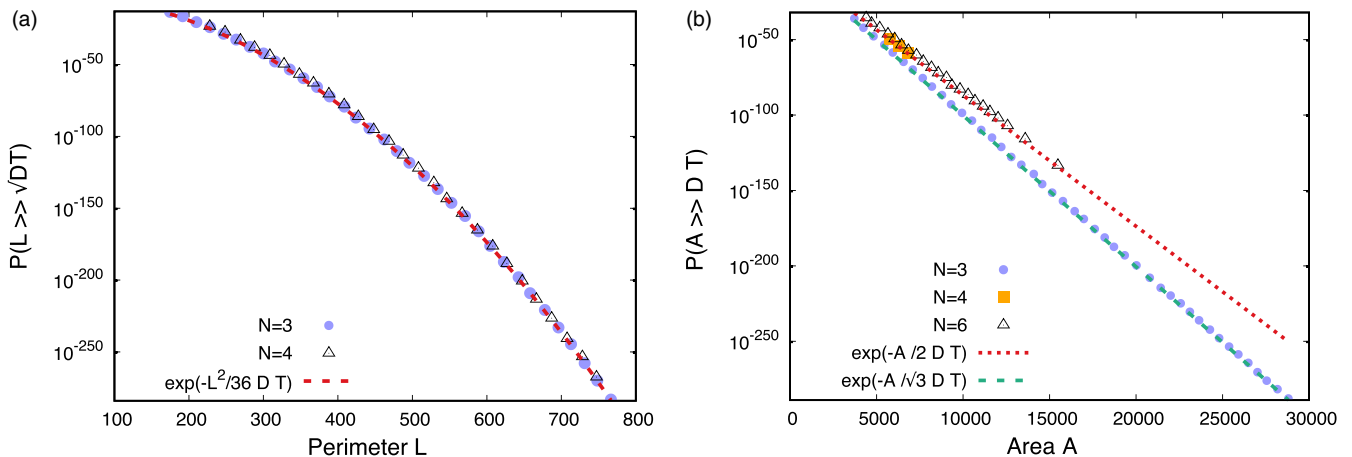


FIG. 9. Right tail distribution of (a) $\mathcal{P}(L)$ and (b) $\mathcal{P}(A)$ for multiple BMs. The markers depict the data of the distributions from Ref. [24] and the dashed and dotted lines denote our theoretical predictions for the distribution tails.

- [1] S. N. Majumdar, Brownian functionals in physics and computer science, *Curr. Sci.* **89**, 2076 (2005).
- [2] F. Schweitzer, *Brownian Agents and Active Particles: Collective Dynamics in the Natural and Social Sciences* (Springer, Berlin, 2003).
- [3] P. Romanczuk, M. Bar, W. Ebeling, B. Lindner, and L. Schimansky-Geier, Active Brownian particles, *Eur. Phys. J. Spec. Top.* **202**, 1 (2012).
- [4] M. C. Marchetti, J. F. Joanny, S. Ramaswamy, T. B. Liverpool, J. Prost, M. Rao, and R. Aditi Simha, Hydrodynamics of soft active matter, *Rev. Mod. Phys.* **85**, 1143 (2013).
- [5] É. Fodor, M. Guo, N. Gov, P. Visco, D. Weitz, and F. van Wijland, Activity-driven fluctuations in living cells, *Europhys. Lett.* **110**, 48005 (2015).
- [6] O. Granek, Y. Kafri, M. Kardar, S. Ro, A. Solon, and J. Tailleur, Inclusions, boundaries and disorder in scalar active matter, [arXiv:2310.00079](https://arxiv.org/abs/2310.00079).
- [7] X. Trepast, M. Wasserman, T. Angelini, E. Millet, D. A. Weitz, J. P. Butler, and J. J. Fredberg, Physical forces during collective cell migration, *Nat. Phys.* **5**, 426 (2009).
- [8] H. Berg and D. A. Brown, Chemotaxis in *Escherichia coli* analysed by three-dimensional tracking, *Nature (Lond.)* **239**, 500 (1972).
- [9] W. Alt, Biased random walk models for chemotaxis and related diffusion approximations, *J. Math. Biol.* **9**, 147 (1980).
- [10] T. Vicsek, A. Czirók, E. Ben-Jacob, I. Cohen, and O. Shochet, Novel type of phase transition in a system of self-driven particles, *Phys. Rev. Lett.* **75**, 1226 (1995).
- [11] J. Tailleur and M. E. Cates, Statistical mechanics of interacting run-and-tumble bacteria, *Phys. Rev. Lett.* **100**, 218103 (2008).
- [12] A. Dhar, A. Kundu, S. N. Majumdar, S. Sabhapandit, and G. Schehr, Run-and-tumble particle in one-dimensional confining potentials: Steady-state, relaxation, and first-passage properties, *Phys. Rev. E* **99**, 032132 (2019).
- [13] M. E. Cates and J. Tailleur, Motility-induced phase separation, *Annu. Rev. Condens. Matter Phys.* **6**, 219 (2015).
- [14] A. B. Slowman, M. R. Evans, and R. A. Blythe, Jamming and attraction of interacting run-and-tumble random walkers, *Phys. Rev. Lett.* **116**, 218101 (2016).
- [15] B. J. Worton, A convex hull-based estimator of home-range size, *Biometrics* **51**, 1206 (1995).
- [16] L. Giuggioli, J. R. Potts, and S. Harris, Animal interactions and the emergence of territoriality, *PLoS Comput. Biol.* **7**, e1002008 (2011).
- [17] Y. Lanoiselée and D. S. Grebenkov, Unraveling intermittent features in single-particle trajectories by a local convex hull method, *Phys. Rev. E* **96**, 022144 (2017).
- [18] E. Dumonteil, S. N. Majumdar, A. Rosso, and A. Zoia, Spatial extent of an outbreak in animal epidemics, *Proc. Natl. Acad. Sci. USA* **110**, 4239 (2013).
- [19] G. Letac, An explicit calculation of the mean of the perimeter of the convex hull of a plane random walk, *J. Theor. Prob.* **6**, 385 (1993).
- [20] J. Randon-Furling, S. N. Majumdar, and A. Comtet, Convex hull of N planar Brownian motions: Exact results and an application to ecology, *Phys. Rev. Lett.* **103**, 140602 (2009).
- [21] S. N. Majumdar, A. Comtet, and J. Randon-Furling, Random convex hulls and extreme value statistics, *J. Stat. Phys.* **138**, 955 (2010).
- [22] A. R. Wade and C. Xu, Convex hulls of random walks and their scaling limits, *Stoc. Proc. Appl.* **125**, 4300 (2015).
- [23] G. Claussen, A. K. Hartmann, and S. N. Majumdar, Convex hulls of random walks: Large-deviation properties, *Phys. Rev. E* **91**, 052104 (2015).
- [24] T. Dewenter, G. Claussen, A. K. Hartmann, and S. N. Majumdar, Convex hulls of multiple random walks: A large-deviation study, *Phys. Rev. E* **94**, 052120 (2016).
- [25] H. Schawe, A. K. Hartmann, and S. N. Majumdar, Convex hulls of random walks in higher dimensions: A large-deviation study, *Phys. Rev. E* **96**, 062101 (2017).
- [26] H. Schawe, A. K. Hartmann, and Satya N. Majumdar, Large deviations of convex hulls of self-avoiding random walks, *Phys. Rev. E* **97**, 062159 (2018).
- [27] H. Schawe and A. K. Hartmann, Large deviations of convex hulls of the “true” self-avoiding random walk, *J. Phys.: Conf. Ser.* **1290**, 012029 (2019).
- [28] A. K. Hartmann, S. N. Majumdar, H. Schawe, and G. Schehr, The convex hull of the run-and-tumble particle in a plane, *J. Stat. Mech.* (2020) 053401.
- [29] S. N. Majumdar, F. Mori, H. Schawe, and G. Schehr, Mean perimeter and area of the convex hull of a planar Brownian motion in the presence of resetting, *Phys. Rev. E* **103**, 022135 (2021).
- [30] P. Singh, A. Kundu, S. N. Majumdar and H. Schawe, Mean area of the convex hull of a run and tumble particle in two dimensions, *J. Phys. A: Math. Theor.* **55**, 225001 (2022).
- [31] R. Eldan, Volumetric properties of the convex hull of an n -dimensional Brownian motion, *Electron. J. Probab.* **19**, 1 (2014).
- [32] Z. Kabluchko and D. Zaporozhets, Intrinsic volumes of Sobolev balls with applications to Brownian convex hulls, *Trans. Am. Math. Soc.* **368**, 8873 (2016).
- [33] V. Vysotsky and D. Zaporozhets, Convex hulls of multidimensional random walks, *Trans. Am. Math. Soc.* **370**, 7985 (2018).
- [34] J. Kampf, G. Last, and I. Molchanov, On the convex hull of symmetric stable processes, *Proc. Am. Math. Soc.* **140**, 2527 (2012).
- [35] B. De Bruyne, O. Benichou, S. N. Majumdar, and G. Schehr, Statistics of the maximum and the convex hull of a Brownian motion in confined geometries, *J. Phys. A: Math. Theor.* **55**, 144002 (2022).
- [36] T. L. Snyder and J. M. Steele, Convex hulls of random walks, *Proc. Am. Math. Soc.* **117**, 1165 (1993).
- [37] A. Goldman, Le spectre de certaines mosaïques poissoniennes du plan et l’enveloppe convexe du pont brownien, *Probab. Theory Relat. Fields* **105**, 57 (1996).
- [38] H. Touchette, Introduction to dynamical large deviations of Markov processes, *Physica A* **504**, 5 (2018).
- [39] A. Akopyan and V. Vysotsky, Large deviations of convex hulls of planar random walks and Brownian motions, *Ann. H. Lebesgue* **4**, 1163 (2021).
- [40] V. Visotsky, The isoperimetric problem for convex hulls and the large deviations rate functionals of random walks, [arXiv:2306.12359](https://arxiv.org/abs/2306.12359).
- [41] H. Touchette, The large deviation approach to statistical mechanics, *Phys. Rep.* **478**, 1 (2009).
- [42] T. Bodineau and B. Derrida, Distribution of current in nonequilibrium diffusive systems and phase transitions, *Phys. Rev. E* **72**, 066110 (2005).

- [43] J. P. Garrahan, R. L. Jack, V. Lecomte, E. Pitard, K. van Duijvendijk, and F. van Wijland, Dynamical first-order phase transition in kinetically constrained models of glasses, *Phys. Rev. Lett.* **98**, 195702 (2007).
- [44] G. Bunin, Y. Kafri, and D. Podolsky, Non-differentiable large-deviation functionals in boundary-driven diffusive systems, *J. Stat. Mech.* (2012) L10001.
- [45] C. P. Espigares, P. L. Garrido, and P. I. Hurtado, Dynamical phase transition for current statistics in a simple driven diffusive system, *Phys. Rev. E* **87**, 032115 (2013).
- [46] Y. Baek and Y. Kafri, Singularities in large deviation functions, *J. Stat. Mech.* (2015) P08026.
- [47] Y. Baek, Y. Kafri, and V. Lecomte, Dynamical symmetry breaking and phase transitions in driven diffusive systems, *Phys. Rev. Lett.* **118**, 030604 (2017).
- [48] Y. Baek, Y. Kafri, and V. Lecomte, Dynamical phase transitions in the current distribution of driven diffusive channels, *J. Phys. A: Math. Theor.* **51**, 105001 (2018).
- [49] T. Nemoto, É. Fodor, M. E. Cates, R. L. Jack, and J. Tailleur, Optimizing active work: Dynamical phase transitions, collective motion, and jamming, *Phys. Rev. E* **99**, 022605 (2019).
- [50] C. Bechinger, R. Di Leonardo, H. Löwen, C. Reichhardt, G. Volpe, and G. Volpe, Active particles in complex and crowded environments, *Rev. Mod. Phys.* **88**, 045006 (2016).
- [51] I. Santra, U. Basu, and S. Sabhapandit, Run-and-tumble particles in two dimensions: Marginal position distributions, *Phys. Rev. E* **101**, 062120 (2020).
- [52] L. Onsager and S. Machlup, Fluctuations and irreversible processes, *Phys. Rev.* **91**, 1505 (1953).
- [53] P. C. Martin, E. D. Siggia, and H. A. Rose, Statistical dynamics of classical systems, *Phys. Rev. A* **8**, 423 (1973).
- [54] M. I. Freidlin and A. D. Wentzell, *Random Perturbations of Dynamical Systems* (Springer, New York, 1984).
- [55] M. I. Dykman and M. A. Krivoglaz, in *Soviet Physics Reviews*, edited by I. M. Khalatnikov (Harwood Academic, New York, 1984), Vol. 5, pp. 265–441.
- [56] R. Graham, in *Noise in Nonlinear Dynamical Systems*, edited by F. Moss and P. V. E. McClintock, Vol. 1 (Cambridge University Press, Cambridge, UK, 1989), p. 225.
- [57] G. Falkovich, K. Gawedzki, and M. Vergassola, Particles and fields in fluid turbulence, *Rev. Mod. Phys.* **73**, 913 (2001).
- [58] A. Grosberg and H. Frisch, Winding angle distribution for planar random walk, polymer ring entangled with an obstacle, and all that: Spitzer-Edwards-Prager-Frisch model revisited, *J. Phys. A: Math. Gen.* **36**, 8955 (2003).
- [59] V. Elgart and A. Kamenev, Rare event statistics in reaction-diffusion systems, *Phys. Rev. E* **70**, 041106 (2004).
- [60] N. Ikeda and H. Matsumoto, in *In Memoriam Marc Yor—Séminaire de Probabilités XLVII*, edited by C. Donati-Martin, A. Lejay, and A. Rouault, Lecture Notes in Mathematics, Vol. 2137 (Springer, Cham, 2015), p. 497.
- [61] T. Grafke, R. Grauer, and T. Schäfer, The instanton method and its numerical implementation in fluid mechanics, *J. Phys. A* **48**, 333001 (2015).
- [62] B. Meerson and N. R. Smith, Geometrical optics of constrained Brownian motion: Three short stories, *J. Phys. A: Math. Theor.* **52**, 415001 (2019).
- [63] N. R. Smith and B. Meerson, Geometrical optics of constrained Brownian excursion: From the KPZ scaling to dynamical phase transitions, *J. Stat. Mech.* (2019) 023205.
- [64] T. Bar and B. Meerson, Geometrical optics of large deviations of Brownian motion in inhomogeneous media, *J. Stat. Mech.* (2023) 093301.
- [65] U. Villanueva-Alcalá, J. R. Nicolás-Carlock, and D. Boyer, Diffusion limited aggregation, resetting and large deviations of Brownian motion, *Mol. Phys.* e2276906 (2023).
- [66] A. Hehl, The Isoperimetric Inequality, <https://www.math.uni-tuebingen.de/ab/GeometrieWerkstatt/IsoperimetricInequality.pdf>.
- [67] J. Weigert, The sagacity of circles: A history of the isoperimetric problem—The work of Jakob Steiner, *Convergence, MathDL, MAA* (2006).
- [68] T. Agranov, B. Meerson, and A. Vilenkin, Survival of interacting diffusing particles inside a domain with absorbing boundary, *Phys. Rev. E* **93**, 012136 (2016).
- [69] F. Di Trapani, T. Franosch, and M. Caraglio, Active Brownian particles in a circular disk with an absorbing boundary, *Phys. Rev. E* **107**, 064123 (2023).
- [70] S. A. Iyaniwura and Z. Peng, Asymptotic analysis and simulation of mean first passage time for active Brownian particles in 1-D, [arXiv:2310.04446](https://arxiv.org/abs/2310.04446).
- [71] R. J. Harris and H. Touchette, Current fluctuations in stochastic systems with long-range memory, *J. Phys. A: Math. Theor.* **42**, 342001 (2009).
- [72] R. J. Harris, Fluctuations in interacting particle systems with memory, *J. Stat. Mech.* (2015) P07021.
- [73] R. L. Jack, Large deviations in models of growing clusters with symmetry-breaking transitions, *Phys. Rev. E* **100**, 012140 (2019).
- [74] R. L. Jack and R. J. Harris, Giant leaps and long excursions: Fluctuation mechanisms in systems with long-range memory, *Phys. Rev. E* **102**, 012154 (2020).
- [75] T. Agranov and G. Bunin, Extinctions of coupled populations, and rare event dynamics under non-Gaussian noise, *Phys. Rev. E* **104**, 024106 (2021).
- [76] N. R. Smith and O. Farago, Nonequilibrium steady state for harmonically-confined active particles, *Phys. Rev. E* **106**, 054118 (2022).
- [77] F. Bouchet, R. Tribe, and O. Zaboronski, Sample-path large deviations for stochastic evolutions driven by the square of a Gaussian process, *Phys. Rev. E* **107**, 034111 (2023).
- [78] N. R. Smith, Nonequilibrium steady state of trapped active particles, *Phys. Rev. E* **108**, L022602 (2023).
- [79] P. J. Paulino, I. Lesanovsky, and F. Carollo, Large deviation full counting statistics in adiabatic open quantum dynamics, [arXiv:2401.11933](https://arxiv.org/abs/2401.11933).
- [80] D. S. Dean, S. N. Majumdar, and H. Schawe, Position distribution in a generalized run-and-tumble process, *Phys. Rev. E* **103**, 012130 (2021).
- [81] P. Pietzonka, K. Kleinbeck, and U. Seifert, Extreme fluctuations of active Brownian motion, *New J. Phys.* **18**, 052001 (2016).
- [82] C. Kurzthaler, C. Devailly, J. Arlt, T. Franosch, W. C. K. Poon, V. A. Martinez, and A. T. Brown, Probing the spatiotemporal dynamics of catalytic Janus particles with single-particle

- tracking and differential dynamic microscopy, *Phys. Rev. Lett.* **121**, 078001 (2018).
- [83] U. Basu, S. N. Majumdar, A. Rosso, and G. Schehr, Long-time position distribution of an active Brownian particle in two dimensions, *Phys. Rev. E* **100**, 062116 (2019).
- [84] Our coefficient $\pi/4$ in Eq. (52) appears to be equal to half the coefficient 1.56 that was numerically observed in Fig. 5(a) of Ref. [25] (the factor of one half comes from their choice of $D = 1/2$). Similarly, the coefficient 5.3 that we inserted in Eq. (53) equals half the coefficient 10.61 that was numerically observed in Fig. 5(c) of Ref. [25].